Dynamic interpretation of resonant x-ray Raman scattering: Ethylene and benzene

F. Hennies,[1,*] S. Polyutov,[2] I. Minkov,[2] A. Pietzsch,[1] M. Nagasono,[1,3,†] H. Ågren,[2] L. Triguero,[4] M.-N. Piancastelli,[5] W. Wurth,[1] F. Gel'mukhanov,[2,‡] and A. Föhlisch[1,§]

[1]*Institut für Experimentalphysik, Universität Hamburg, Luruper Chaussee 149, 22761 Hamburg, Germany*

[2]*Theoretical Chemistry, Royal Institute of Technology, AlbaNova University Center, 106 91 Stockholm, Sweden*

[3]*Department of Materials Science and Engineering, Kyoto University, Sakyo-ku, 606-8501 Kyoto, Japan*

[4]*KTH Syd, Royal Institute of Technology, Campus Haninge, 136 40 Haninge, Sweden*

[5]*Department of Physics, Uppsala University, Box 530, 751 21 Uppsala, Sweden*

(Received 4 May 2007; published 18 September 2007)

We present a dynamic interpretation of resonant x-ray Raman scattering where vibrationally selective excitation into molecular resonances has been employed in comparison with excitation into higher lying continuum states for condensed ethylene and benzene as molecular model systems. In order to describe the purely vibrational spectral loss features and coupled electronic and vibrational losses the one-step theory for resonant soft x-ray scattering is applied, taking multiple vibrational modes and vibronic coupling into account. The scattering profile is found to be strongly excitation energy dependent and to reflect the intermediate states dynamics of the scattering process. In particular, the purely vibrational loss features allow one to map the electronic ground state potential energy surface in light of the excited state dynamics. Our study of ethylene and benzene underlines the necessity of an explicit description of the coupled electronic and vibrational loss features for the assignment of spectral features observed in resonant x-ray Raman scattering at polyatomic systems, which can be done in both a time independent and a time dependent picture. The possibility to probe ground state vibrational properties opens a perspective to future applications of this photon-in-photon-out spectroscopy.

DOI: 10.1103/PhysRevA.76.032505 PACS number(s): 33.20.Fb, 33.20.Rm, 33.20.Tp, 33.50.Dq

I. INTRODUCTION

Resonant x-ray Raman scattering is used to probe stationary and dynamic properties of matter [1–4]. As a photon-in-photon-out method it provides a large penetration depth and is applicable to matter in all aggregate states and external fields. The resonant inelastic x-ray scattering (RIXS) probes electronic and nuclear (vibrational) inelastic loss processes. Most work so far has focused on the investigation of the atom specific and chemical state selective electronic structure.

The absorption and emission of soft x-ray photons are governed by the dipole selection rules. Spectroscopy based on these processes therefore provides a clear polarization anisotropy, providing information on symmetry and orientation of electronic states. Soft x-ray spectroscopies are element and chemical state selective, since they involve transitions from core orbitals. In the resonant x-ray Raman scattering process, a particular intermediate core-excited state of defined symmetry is prepared by selective excitation, thus enhancing the former properties [5]. In a coherent one-step scattering picture the selection rules of excitation and decay converge to a Raman selection rule. The scattering process is then ruled by the symmetry of the system's total wave function including all nuclear and electronic contributions.

Resonant x-ray Raman scattering has been applied to a wide range of systems, including crystalline solids, surface adsorbates, and free molecules [2,4,6,7]. Spectra of crystalline solids have been interpreted based on the description of electronic states in band structure calculations [4]. Utilizing the atom specificity, it has been possible to examine the electronic density of states (DOS) projected on the contributions of different atoms in a compound system. This has been extremely useful in the case of surface adsorbates [1,5,8,9], where the electronic structure of the adsorbed molecule can be investigated suppressing the vast majority of substrate contributions. Combined with the symmetry selectivity, this has allowed one to study the formation of the surface chemical bond in great detail. For the case of adsorbates on metals it has been shown that the spectral profile can fully be described in the so-called "ground state interpretation" [8]. Here, the energy distribution of the scattering spectra is directly derived from the difference of ground state orbital energies, e.g., obtained from density functional theory (DFT) calculations. The selectivity of the excitation is explicitly taken into account in this model, modulating the intensity distribution of the spectral profile [9]. In this pure electronic interpretation, the selection rules for the scattering process are applied only to the electronic part of the systems total wave function.

The influence of nuclear motion on RIXS spectra has been discussed as phonon side bands in the case of diamond and graphite [10,11]. The vibrational loss processes are identified in an asymmetric tail of the recombination emission. For molecules, the shaping of the RIXS bands due to lifetime-vibrational interference has been demonstrated

*Corresponding author. Present address: MAX-lab, Lund University, Box 118, 221 00 Lund, Sweden. franz@hennies.org

†Present address: RIKEN/XFEL Project, Head office, Kouto 1-1-1, Sayo, Hyogo 679-5148, Japan.

‡Permanent address: Institute of Automation and Electrometry, 630090 Novosibirsk, Russia.

§Corresponding author. alexander.foehlisch@desy.de

[12,13]. In this case, the core hole lifetime broadening is of the same order of magnitude as the vibrational spacing in the core excited intermediate state which gives rise to channel interference in the scattering process. In these works, the vibrational effects are discussed as additional contributions to the electronic states probed. In a general treatment of resonant x-ray Raman scattering, always the changes in the combined nuclear and electronic contributions to the systems total wave function have to be considered. In the scattering profile of molecules, therefore, strong deviations from a model accounting only for electronic symmetry selection rules have been observed and discussed as bond length dependent core hole localization [14] and breaking of electronic symmetry [15,16]. Nevertheless, here too, only the influence of these effects on the electronic spectral structure is discussed.

In two recent publications [17,18], the electronic and geometric structure of liquids has been investigated with resonant inelastic x-ray scattering. In both studies, the spectral profile has been interpreted on the basis of calculations of the ground state electronic structure in the adiabatic limit disregarding vibrational effects [19]. In particular, the low count rate achieved for x-ray emission on light elements in todays setups has for a long time not allowed one to interpret the scattering spectra of a system completely in all aspects of vibrational band formation, interference effects, and vibronic coupling. We have recently demonstrated that in the case of molecules, vibrational influences on the spectral profile cannot only be considered as additional effects in the electronic features visible in the spectra, but have to be understood as constituting the spectral profile [20].

In the present paper, we systematically develop a complete interpretation of RIXS on condensed ethylene and benzene based on the consideration of electronic structure, nuclear dynamics, and vibronic coupling. We will show how RIXS probes the electronic ground state potential energy surface in light of the excited state nuclear dynamics as an atom specific, chemical sensitive Raman spectroscopy.

II. EXPERIMENTAL SETUP

The experiments have been performed at the Swedish National Laboratory MAX-lab in Lund at beamline I511-1. The beamline is equipped with an end station operated in UHV dedicated for x-ray absorption spectroscopy (XAS), photoelectron spectroscopy (XPS), and x-ray emission spectroscopy (XES) measurements on adsorbate, surface and bulk samples. The station consists of a preparation chamber operated at a base pressure of low 10^{-10} torr connected to an analysis chamber (at mid 10^{-11} torr). The analysis chamber is equipped with a Scienta SES 200 hemispherical electron analyzer for XPS and partial electron yield XAS measurements. XES is detected with a grazing incidence soft x-ray fluorescence spectrometer [2].

For the XAS, the excitation bandwidth was set to ~35 meV. For the excitation of the resonant x-ray scattering spectra, the bandwidth of the incident photons was set to ~100 meV in the case of the ethylene measurements and ~250 meV in case of benzene. The overall instrumental resolution of the x-ray emission spectra was ~400 meV [full width at half maximum (FWHM)], as determined by measuring reflected light on a silicon substrate in the first order.

The x-ray absorption spectra have been recorded with the Scienta Analyzer in constant final state mode with a pass energy of 500 eV. In the case of the benzene measurements, we detected electrons in an energy window of 50 eV width centered around the carbon KLL auger. The ethylene multilayer was found to charge too much during irradiation with synchrotron light to be able to detect the carbon auger properly. Therefore, we have chosen to measure the yield of low energy electrons in an energy range of ($120\ \text{eV} \leq E_{Kin.} \leq 168\ \text{eV}$) where charge effects were found not to disturb the absorption spectra. For normalization purposes we measured the photon flux simultaneously with a reference gold mesh. The partial yield spectra shown here have been normalized by division by the flux signal. The x-ray emission spectra have not further been treated except for the correction to a calibrated energy scale. A total energy calibration of the incoming photon energy has been performed by exciting Si $2p$ electrons with first- and second-order light passing the monochromator.

The samples were prepared by exposing a silicon substrate at a temperature $T \leq 100$ K to gaseous benzene ($T \leq 25$ K for ethylene, respectively) at a pressure of $P = 5 \times 10^{-7}$ torr for 200 s (100 L). Before dosing the high purity liquid benzene was further purified by repeated freeze-pump-thaw cycles, gaseous ethylene (purity 2.8) was directly used. Cleanliness of the gases was assured by checking with a mass spectrometer. Physisorbed benzene has a sticking coefficient near 1 [21], thus, our preparation conditions lead to the formation of a ~100 ML thick multilayer of benzene with a randomly tilted orientation of the molecules [21]. Ethylene at the used temperatures forms bulk crystalline structures [22]. We do not account for any angular anisotropies here, since the comparison between our XAS data and XAS measured on statistically distributed gas-phase ethylene [23] shows no difference in the resonance region.

To avoid beam damage, we scanned the samples during the measurements. Each spectrum comprises a 15–30 min measurement time (longer measurement times for the detuned spectra). The sample was scanned with a rate of $v_x = 5\ \mu\text{m/s}$ at a spot size at sample position of estimated $\Delta x = 50\ \mu\text{m}$ by $\Delta z = 400\ \mu\text{m}$ (FWHM). The beamline delivers a photon flux [24] of approx. 10^{11} photons/s at the chosen energy and bandwidth. Photon-induced decomposition has been reported for benzene [25] and ethylene [26], but no cross section data appears to be available. However, we found no indication of beam induced processes in the condensed layers at the irradiation rates used, as the XE spectra did not change during the exposure to the synchrotron light. Furthermore, the XE spectra measured here resemble data reported from gas-phase measurements [14] or older measurements in the condensed phase with less statistics [16] and, thus, presumably lower exposure.

III. METHODICAL FRAMEWORK

The resonant x-ray scattering profile can be divided into two qualitatively different contributions, namely, the partici-

pator and the spectator band. In the participator band the final electronic state f reached in the scattering process equals the initial electronic state, which is in the present work always the ground state 0. In the spectator band final and initial electronic state differ from each other ($f \neq 0$).

It is common and suitable in some cases to refer to these different bands as "inelastic" (RIXS) and "elastic" (REXS) scattering. However, such a definition is not valid in a strict sense, because even the participator band includes inelastic loss processes due to scattering into excited vibrational levels of the electronic ground state. RIXS is governed by a Raman selection rule operating on the total electronic and vibrational wave function of the system [3,27]. If the Born-Oppenheimer (BO) approximation is valid, electronic and nuclear degrees of freedom can be separated. In this case the scattering process follows purely electronic selection rules as well [3,28,29]. Selection rules operating isolated on electronic and nuclear subsystems can be broken when the BO approximation ceases to be valid. The breakdown of purely electronic selection rules happens in the almost degenerated core excited states of the symmetrical molecules studied here. This motivates us to develop a formalism which takes the symmetry breaking of the electronic subsystem during the scattering through close lying core excited states into account.

A. Kramers-Heisenberg formalism

We investigate the resonant inelastic scattering of an x-ray photon at a molecule initially in the electronic and vibrational ground state $|0,0\rangle$.

The absorption of the incident photon with energy ω and polarization vector $\mathbf{e}$ promotes the scatterer into an intermediate multimode vibrational state $|\nu_i\rangle = \Pi_q |\nu_{i,q}\rangle$ of the core excited electronic state i, coherently followed by the decay of the excited state into the vibrational state $|\nu_f\rangle = \Pi_q |\nu_{f,q}\rangle$ of the final electronic state f under emission of a second photon $(\omega_1, \mathbf{e}_1)$. Here $\nu_i = (\nu_{i,1}, \nu_{i,2}, \ldots, \nu_{i,N})$ is the vector of vibrational quantum numbers $\nu_{i,q}$ of different modes q of electronic state i. The spectral distribution of the emitted photon ω_1 is accordingly given by the differential cross section for resonant x-ray scattering [3] containing the spectral function of the incident radiation Φ and the scattering amplitude F_{ν_f},

$$\sigma(\omega, \omega_1) = \sum_{f,\nu_f} |F_{\nu_f}|^2 \Phi(\omega_1 - \omega + \omega_{f\nu_f,00} + \omega^e_{f0}, \gamma). \quad (1)$$

The spectral function $\Phi(\omega - \omega_0, \gamma)$ centered at ω_0 with linewidth γ (full width at half maximum FWHM, as all comparable values in this work) describes the energy distribution of the spectral features. For each final electronic vibrational state $|f, \nu_f\rangle$, the spectral line occurs at an energy difference $\Delta\omega_1 = \omega_1 - \omega$ equaling the sum of the electronic and vibrational excitations $\omega^e_{f0} + \omega_{f\nu_f,00}$ present in the final state. Here, ω^e_{f0} denotes the difference between the lowest vibrational levels of the electronic final and ground state, $\omega_{j\nu_j,i\nu_i} = \epsilon_{j\nu_j} - \epsilon_{i\nu_i}$, and $\epsilon_{j\nu_j}$ is the vibrational energy of the ν_j multimode vibrational state of the j electronic level.

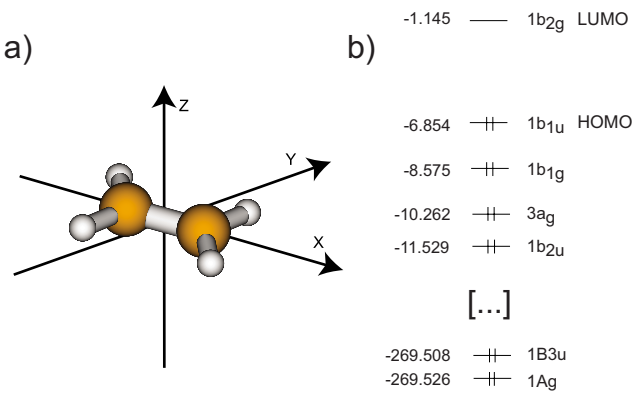

FIG. 1. (Color online) (a) The ethylene molecule with the coordinate system used in our work. (b) The energy levels of ethylene involved in the scattering process (in eV). The two inner shell orbitals ($2a_g$ and $2b_{3u}$) are omitted as irrelevant.

B. Multimode scattering amplitude and vibronic coupling

We outline here the resonant x-ray scattering theory for polyatomic molecules having two equivalent carbon atoms as it is the case for ethylene (Fig. 1). As it was already mentioned, the separation of electronic and nuclear degrees of freedom, simply spoken the BO approximation, breaks down in core excited states of symmetric molecules [30]. This is generally possible in presence of quasidegenerate core levels, more precisely, when the spacing Δ between core levels of different parities is small in comparison with the vibronic coupling (VC) interaction V: $\Delta \ll |V|$. The excitation of asymmetric vibrational modes Q_A mixes core excited states of different parities. This nonadiabatic mixing leads to a localization of core holes [3,30,31] and, hence, to the violation of pure electronic selection rules in x-ray Raman scattering.

In the particular case of an ethylene molecule considered here the total scattering amplitude given by the Kramers-Heisenberg formula [3,32] is accordingly the sum of the scattering amplitudes through the core excited states localized at each single carbon atom 1 and 2 (see Fig. 2),

$$F_{\nu_f} = F^{(1)}_{\nu_f} + F^{(2)}_{\nu_f},$$

$$F^{(n)}_{\nu_f} = \sum_{\nu_i} \frac{(\mathbf{e}_1 \cdot \mathbf{d}_{f,n})(\mathbf{e} \cdot \mathbf{d}_{i,n}) \langle \nu_f | \nu_i, n \rangle \langle \nu_i, n | 0_0 \rangle}{\omega - \omega^e_{i0} - \omega_{i\nu_i,00} + \imath\Gamma}. \quad (2)$$

F_{ν_f} is here stated for the limit of small bandwidth excitation and for the case of a single vibrational mode. $\mathbf{d}_{i,n} = \langle \psi_i | \mathbf{r} | 1s_n \rangle$ and $\mathbf{d}_{f,n} = \langle \psi_f | \mathbf{r} | 1s_n \rangle$ are the electronic transition dipole moments of core excitation and decay of the nth carbon in one-electron approximation. The total Franck-Condon (FC) amplitude of the scattering for a molecule with multiple vibrational modes contains the product of the FC amplitudes

$$\langle \nu_f | \nu_i, n \rangle \langle \nu_i, n | 0_0 \rangle = \prod_q \langle \nu_{f,q} | \nu_{i,q} \rangle \langle \nu_{i,q} | 0_{0,q} \rangle \quad (3)$$

of all vibrational modes q.

If the lifetime broadening Γ is comparable to the energy spacing $\omega_{i\nu'_i,i\nu_i}$ of the vibrational intermediate states ν_i, the

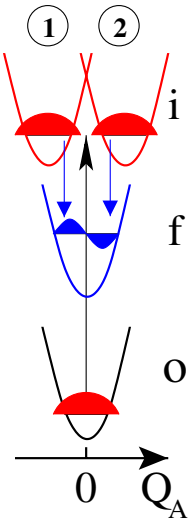

FIG. 2. (Color online) Scheme of transitions for ethylene. Vibronic coupling through the asymmetric mode b_{3u} (see text) localizes the core excited states at carbon atom 1 or carbon 2. The scattering now happens through these interfering scattering channels.

scattering occurs through different intermediate vibrational levels ν_i and give rise to channel interference [33]. We will show in the following that interference effects predominantly determine the spectral appearance of resonant x-ray Raman spectra.

Ethylene belongs to the D_{2h} symmetry group, the ground state electronic configuration is

$$\text{Core: } (1a_g)^2(1b_{3u})^2 = \psi_{\text{core}},$$

$$\text{Valence: } (2b_{3u})^2(1b_{2u})^2(3a_g)^2(1b_{1g})^2(1b_{1u})^2.$$

In Fig. 1, we show the molecule and its energy levels in the reference frame used in this work. Ethylene has two near degenerate core orbitals in delocalized representation, here referred to as ψ_{core}. They result from the linear combination of the C $1s$ atomic orbitals. The highest occupied molecular orbital (HOMO) $(1b_{1u})$ has π character. The lowest unoccupied molecular orbital (LUMO) with π^* character is the $(1b_{2g})$ orbital. The role of the VC is studied here in detail when the photon frequency is tuned near the LUMO $\psi_i = 1b_{2g}$ of *gerade* symmetry. The emission transitions from occupied MOs $\psi_f = 1b_{1u}$, $1b_{1g}$, $3a_g$, and $1b_{2u}$ form the fluorescence spectrum discussed here.

Localized core orbitals

$$1s_{1,2} \approx \frac{1}{\sqrt{2}}(1b_{3u} \pm 1a_g) \tag{4}$$

form symmetry adapted delocalized *gerade* and *ungerade* core orbitals $1a_g$ and $1b_{3u}$.

The partial scattering amplitudes $F^{(1)}_{\nu_f}$ and $F^{(2)}_{\nu_f}$ differ from each other by the FC amplitudes $\langle \nu_f | \nu_i, n \rangle \langle \nu_i, n | 0_0 \rangle$ which are different for carbon $n=1$ and carbon $n=2$. This difference arises since asymmetric vibrational modes localize the core holes. Particularly, $\langle \nu_f | \nu_i, 1 \rangle \langle \nu_i, 1 | 0_0 \rangle \neq \langle \nu_f | \nu_i, 2 \rangle \langle \nu_i, 2 | 0_0 \rangle$ because the minima of the potential curve of the localized core excited states are shifted along the coordinate Q_A of the asymmetric mode accounting for the localization in opposite directions relative to the equilibrium position (Fig. 2). It is instructive to express the localized core orbitals $1s_{1,2}$ by the delocalized orbitals $1a_g$ and $1b_{3u}$ (4) to see the role of the selection rules in the x-ray Raman scattering.

We now extract the electronic transition moments from the scattering amplitude and average the cross section (1) over molecular orientations and over the polarization vector of the emitted photon. The cross section then reads

$$\sigma(\omega, \omega_1) = \sum_{f,\nu_f} \zeta_{f0} |\mathcal{F}_{\nu_f}|^2 \Phi(\omega_1 - \omega + \omega_{f\nu_f,00} + \omega^e_{f0}, \gamma) \tag{5}$$

with the anisotropy factor

$$\zeta_{f0}(\theta) = \frac{d^2_{fi} d^2_{i0}}{9} \left(1 + \frac{1}{10}(3\cos^2\varphi_{f0} - 1)(1 - 3\cos^2\chi) \right), \tag{6}$$

where $\chi = \angle(\mathbf{k}_1, \mathbf{e})$ is the angle between the wave vector $\mathbf{k}_1$ of the emitted photon and the polarization vector of the incident photon $\mathbf{e}$, φ_{f0} is the angle between the dipole moments of the core excitation, $\mathbf{d}_{i0}$, and emission, $\mathbf{d}_{fi}$, transitions in delocalized representation. In the studied case of the ethylene molecule being excited into the LUMO they become $\mathbf{d}_{i0} = \langle 1b_{2g} | \mathbf{r} | 1b_{3u} \rangle$ and

$$\mathbf{d}_{fi} \equiv \begin{cases} \langle \psi_f | \mathbf{r} | 1b_{3u} \rangle, & \text{if } f = g, \\ \langle \psi_f | \mathbf{r} | 1a_g \rangle, & \text{if } f = u. \end{cases} \tag{7}$$

In the scattering amplitude $\mathcal{F}_{\nu_f}$ we now have to distinguish the scattering through symmetric vibrational modes (S) from scattering through asymmetric vibrational modes (A). Contrary to the asymmetric modes with $\Lambda^A_1 \neq \Lambda^A_2$, the FC amplitudes of symmetric modes Λ^S are the same for the scattering channels $n=1$ and $n=2$. Due to this, the FC amplitude Λ^S can be extracted from the sum over $n=1,2$ [3,34,35],

$$\mathcal{F}_{\nu_f} \approx \frac{1}{2} \sum_{\nu_i} \frac{\Lambda^S(\Lambda^A_1 + \mathcal{P}_f \Lambda^A_2)}{\omega - \omega^e_{i0} - \omega_{i\nu_i,00} + i\Gamma/2},$$

$$\Lambda^S = \prod_{q \not\subseteq A} \langle \nu_{f,q} | \nu_{i,q} \rangle \langle \nu_{i,q} | 0_{0,q} \rangle,$$

$$\Lambda^A_n = \prod_{q \subseteq A} \langle \nu_{f,q} | \nu_{i,q}; n \rangle \langle \nu_{i,q}; n | 0_{0,q} \rangle, \quad n = 1,2. \tag{8}$$

Here, $|\nu_{i,q}; n\rangle$ is the vibrational wave function of the q asymmetric mode in the core excited state with the core hole localized on the n atom (given for two equivalent atoms). $\mathcal{P}_f$ is the parity of the final electronic state ν_f,

$$\mathcal{P}_f = \begin{cases} 1, & f = g, \\ -1, & f = u. \end{cases} \tag{9}$$

Equation (8) displays the ordinary electronic selection rules for resonant x-ray Raman scattering, namely, quenching of the scattering into *ungerade* final states, $\mathcal{F}_{\nu_f} = 0$, when $\Lambda^A_1 = \Lambda^A_2$. The vibronic coupling mediated by asymmetric vi-

TABLE I. Excited state parameters for ethylene: vertical excitation energy (ω^v), transition dipole moments (d), cos φ_{f0}, where φ_{f0} is the angle between the transition dipole moments of core excitation and decay, and the anisotropy factor ζ_{f0}. $1b_{2g}$ denotes the core excited state produced by the $1s\rightarrow$ LUMO transition, while the rest of the states are valence excited and produced by a decay transition from an orbital with the respective symmetry to the core hole. Only nonzero components of the transition dipole moment are listed: d^z, d^y, d^x.

	ω^v (eV)	d (a.u.)	cos φ_{f0}	ζ_{f0} (10^{-6} a.u.^{2})
$1b_{2g}$	283.92	0.0733^z	1	2.558
$1b_{1u}$	278.27	0.0765^z	-1	2.788
$1b_{1g}$	276.55	0.0586^y	0	2.254
$3a_g$	274.97	0.0822^x	0	4.435
$1b_{2u}$	273.69	0.0658^y	0	2.839

brational modes breaks these selection rules because there $\Lambda_1^A \neq \Lambda_2^A$ due to opposite shifts of the core excited potentials caused by localization of the core holes (Fig. 2). This effect of the electronic symmetry breaking caused by nuclear motion is a dynamical effect and strongly depends on the duration of the scattering, determined by the detuning of the incident photon energy from the absorption resonance of the scatterer (complete discussion in Sec. V).

C. Computational details

We have simulated the spectra utilizing strict *ab initio* methods based on the wave packet technique described in [3,34,36] and the theoretical description given here. Computations of the absorption and emission transition dipole moments from the C 1*s* were performed in the dipole approximation and have been done within the framework of the density functional theory (DFT) using the StoBe code [37] and employing the PW91 density functional for both exchange and correlation contributions. The transition energies were taken directly from the ground state Kohn-Sham orbital energies. The gradients of the core excited potential along normal modes were computed using an effective core potential for the nonexcited carbon, thus effectively localizing the core hole. The core excited center was described by a rather large IGLO-III basis set [34,36].

The resonant x-ray scattering spectral profile was computed making use of the scattering cross section [Eq. (5)] and the Franck-Condon amplitude including the treatment of the vibronic coupling [Eq. (8)]. The spectral function $\Phi(\omega_1 - \omega, \gamma)$ was modeled by a Gaussian with FWHM γ=0.1 eV. In the simulations we used the experimental angle between the wave vector $\mathbf{k}_1$ of the emitted photon and the polarization vector of the incident photon $\mathbf{e}$, χ=35.3°. The lifetime broadening (FWHM) of the core excited state was set to Γ =0.1 eV, corresponding to the estimated carbon 1*s* core hole lifetime for ethylene [38,39]. Transition dipole moments and energies for ethylene are collected in Table I.

The Franck-Condon amplitudes were computed in harmonic approximation making use of the gradient $F_{iq} = dE_i/Q_q$ along the vibrational mode q in the equilibrium geometry of the ground state. The changes of the vibrational frequencies under electronic excitations are ignored in our simulations. We have only taken into consideration those four vibrational modes which were found to give significant contribution to the XAS and RIXS spectra (see Table II). The scattering amplitude is calculated taking into account excitation of each mode up to 8 and 11 vibrational levels for core excited and final states, respectively.

The energy scale of the computed spectra was adjusted with respect to the experimental values by a constant offset to match the top of the absorption resonance.

IV. RESULTS AND ANALYSIS

We first measured the absorption spectra in the region of the carbon *K* edge to characterize the scattering intermediate state for ethylene and benzene. In the following, we performed RIXS at both molecules with selective excitation of defined intermediate states.

A. Ethylene

In Fig. 3, we show carbon *K*-edge x-ray absorption spectroscopy (XAS) of condensed ethylene and theoretical simulations in the resonance region. The spectrum shows an absorption resonance at 284.37 eV with fine structure. The resonance is clearly separated from a continuum region at higher energies with two broad resonances at 287.8 eV and 288.68 eV. We will at first discuss the resonance and turn to the higher energy states later. We compared the spectra with high-resolution XAS of ethylene measured in the condensed phase [40] and in the gas phase [23]. The first resonance represents the C $1s \rightarrow \pi^*(1b_{2g})$ transition, i.e., excitation into

TABLE II. Vibrational normal modes excited in x-ray absorption and x-ray Raman scattering of ethylene. ω_q denotes the vibrational frequency, $F_{iq}=dE_i/dQ_q$ represents the gradient along the particular mode for the vertical core excitation $1b_{2g}$ state and for decay to four final states: $|1b_{1u}^{-1}1b_{2g}\rangle$, $|1b_{1g}^{-1}1b_{2g}\rangle$, $|3a_g^{-1}1b_{2g}\rangle$, $|1b_{2u}^{-1}1b_{2g}\rangle$. The b_{3u} mode vibronically couples core excited states of *gerade* and *ungerade* symmetry.

			F_{iq} (10^{-3} a.u.)				
q mode	symm.	ω_q (eV)	$1b_{2g}$	$1b_{1u}$	$1b_{1g}$	$3a_g$	$1b_{2u}$
3 (C-H sym. stretch)	a_g	0.379	1.498	0.624	−0.881	0.063	−0.784
4 (C-H asym. stretch)	b_{3u}	0.379	1.098	−0.023	0.031	0.039	0.007
5 (C-C stretch)	a_g	0.207	−0.498	−1.424	0.152	−2.127	−0.522
7 (H-C-H scissoring)	a_g	0.165	−0.106	−0.701	−0.750	0.420	−1.527

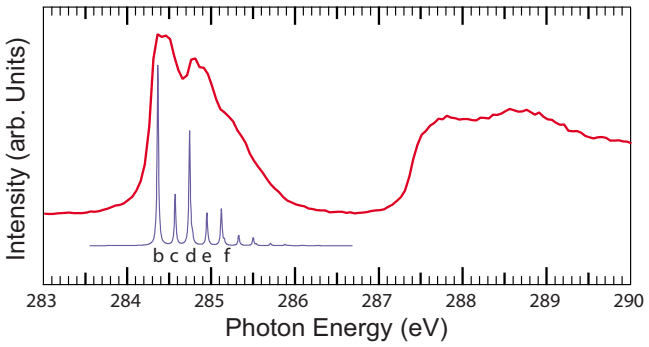

FIG. 3. (Color online) X-ray absorption spectrum of condensed ethylene. Thick line, experiment; thin line, simulation in the region of the π^* resonance. Four modes are calculated (see Table II): (b) $0\rightarrow 0$; (c) $\nu_5(0\rightarrow 1)$; (d) 60%: $\nu_3(0\rightarrow 1)/40\%$: $\nu_4(0\rightarrow 1)$; (e) 60%: $[\nu_5(0\rightarrow 1)+\nu_3(0\rightarrow 1)]/40\%$: $[\nu_5(0\rightarrow 1)+\nu_4(0\rightarrow 1)]$; (f) $\nu_3(0\rightarrow 1)+\nu_4(0\rightarrow 1)$.

an electronic state $|\psi_{\text{core}}^{-1}1b_{2g}\rangle$. The appearance of this feature is identical in the gas phase and condensed phase measurements. This affirms that the condensed ethylene in the region of the π^* resonance can act as a model for a free molecule. The resonance fine structure stems from vibrational excitations. We also show our simulations of the XAS. Our theoretical simulation has shown that only four vibrational modes are active in the scattering process (see Sec. III C). According to our simulations and in agreement with Gadea *et al.* [23], we can assign the vibrational states: Maximum (b) corresponds to the zero-phonon line $0\rightarrow 0$, (c) to the one-phonon excitation of an a_g C-C symmetric stretch mode, (d) contains overlapping one-phonon excitations of a b_{3u} C-H asymmetric stretch mode and a a_g C-H symmetric stretch mode, (e) contains the overlapping two-phonon excitations $[(0\rightarrow 1)$ C-C symmetric $\otimes$ $(0\rightarrow 1)$ C-H symmetric$]$ and $[(0\rightarrow 1)$ C-C symmetric $\otimes$ $(0\rightarrow 1)$ C-H asymmetric$]$, and (f) the two-phonon transition $[(0\rightarrow 1)$ C-H symmetric $\otimes$ $(0\rightarrow 1)$ C-H asymmetric$]$ (see caption of Fig. 3).

We have measured RIXS for selective excitation into the vibrational states of the π^* resonance and performed RIXS simulations at the according energies. The resonant scattering with excitation into the π^* resonance is presented in Fig. 4. Panel 1 of Fig. 4 contains the XA spectrum from Fig. 3 in the π^* resonance region, with the vibrational progression assigned in the plot. Panel 2 of Fig. 4 contains experimental RIXS spectra, taken at excitation energies indicated in the XA spectrum by the horizontal lines. Panel 3 of Fig. 4 contains the corresponding simulations. We convoluted the simulated spectra with a Gaussian of FWHM=0.4 eV to mimic the spectral distribution of the incident photon and the instrumental broadening. In addition, we show the computations with only 0.1 eV broadening to illustrate the underlying spectral structure. The RIXS spectra are displayed on an energy loss scale corresponding to the energy difference between outgoing and incoming photon.

The spectral profile consists of the two above discussed distinct bands, namely, the spectator $(-14\text{ eV}\lesssim\Delta\omega_1\lesssim -5\text{ eV})$ and the participator $(\Delta\omega_1\approx 0)$. The experimental RIXS data and the theoretical simulations both show strong excitation energy dependence. We first turn to the experi-

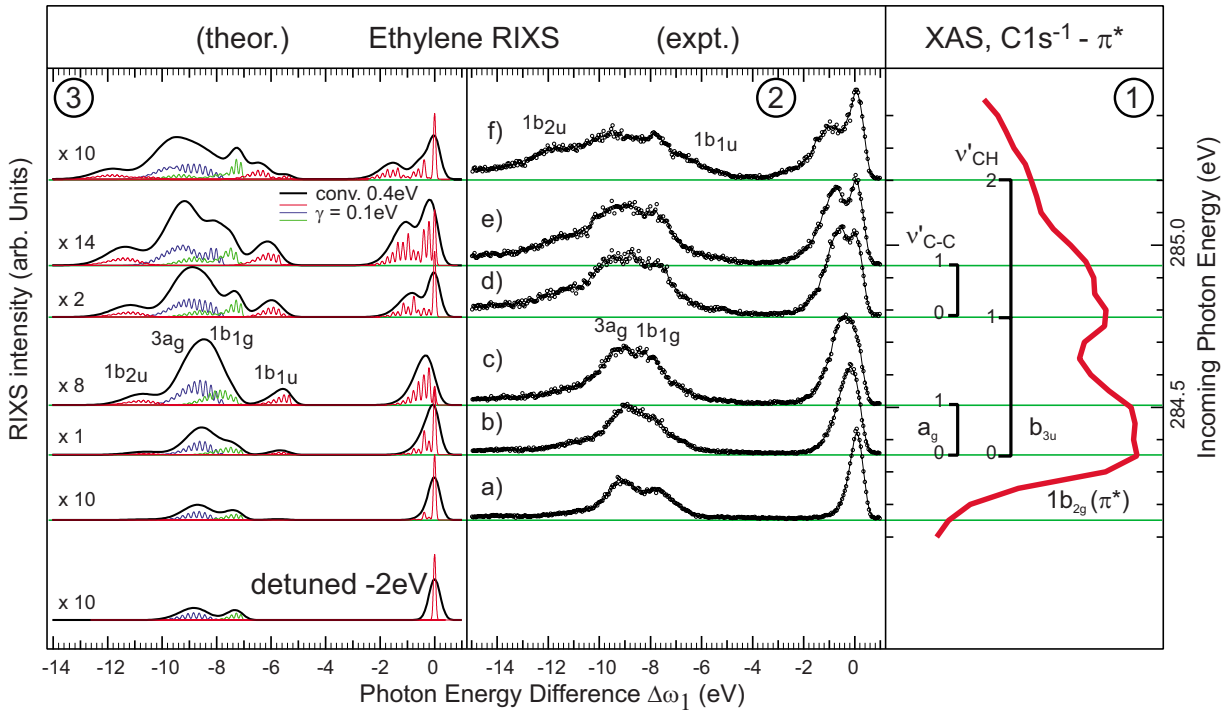

FIG. 4. (Color online) RIXS of ethylene at the C *K* edge in the region of the C $1s\rightarrow\pi^*$ resonance. Panel (1): Absorption spectrum with partly assigned vibrational states; (2): RIXS spectra (exp.) with excitation at the energies indicated; (3): Simulated RIXS at the according energies. RIXS spectra are plotted vs the energy difference of outgoing and incoming photon $\Delta\omega_1=\omega_1-\omega$. The experimental spectra are arbitrarily scaled to equal maximum height.

mental data (Fig. 4, panel 2). When exciting below the resonance energy (a), an isolated, nearly symmetric peak centered at 0 eV energy loss with FWHM of 0.4 eV and two broad features at −7.8 eV and −9.4 eV can be seen. The feature centered at 0 eV is the participator band which corresponds to scattering into the electronic ground state ($|0\rangle \rightarrow |\psi_{\mathrm{core}}^{-1} 1b_{2g}\rangle \rightarrow |0\rangle$). The features at −7.8 eV and −9.4 eV belong to the spectator band and correspond to scattering into electronically valence excited final states ($|0\rangle \rightarrow |\psi_{\mathrm{core}}^{-1} 1b_{2g}\rangle \rightarrow |3a_g^{-1} 1b_{2g}\rangle$ and $|1b_{1g}^{-1} 1b_{2g}\rangle$). We have tentatively assigned the corresponding states following our simulations and in agreement with Gunnelin *et al.* [14] and Triguero *et al.* [41] as marked in the figure.

When increasing the excitation energy, two qualitatively different effects can be observed (see Fig. 4): a broadening of the features that is asymmetric toward lower energies, and the appearance of additional features. After resonant excitation on top of the electronic resonance (b), the peak at 0 eV becomes asymmetric toward lower energies. Exciting into the higher vibrational resonances [4(c)–4(g)], this feature splits into two contributions, one staying at 0 eV and one moving toward lower energies with increasing excitation energy. The lower energy fraction decreases in intensity with increasing excitation energy compared to the part at 0 eV. The features representing the valence electronically excited final states $|1b_{1g}^{-1} 1b_{2g}\rangle$ and $|3a_g^{-1} 1b_{2g}\rangle$ broaden and merge when increasing the excitation energy to the electronic resonance (b) and further to the first vibrational level (c). They become increasingly asymmetric and their center of gravity moves toward lower energies. Increasing the incident photon energy to higher vibrational levels (d)–(f) not only changes the appearance of the states visible with detuned excitation: Additional features show up, assigned to the valence excited final states $|1b_{1u}^{-1} 1b_{2g}\rangle$ and $|1b_{2u}^{-1} 1b_{2g}\rangle$. These features gain intensity with increasing excitation energy.

Our strictly *ab initio* simulations (panel 3 of Fig. 4) of the resonant x-ray scattering at ethylene agree well with the experimental spectra, both in the participator region corresponding to scattering into the electronic ground state as in the spectator region with valence electronically excited final states. By comparison of experiment and theory we see that the experimentally observed spectral distribution is composed by bands of close lying vibrational loss features. As a function of excitation energy these bands broaden and the intensity is strongly redistributed within each band. They move their center of gravity and even shape a bimodal structure in some states. The single vibrational peaks visible in the simulations cannot be resolved in the experiment. Nevertheless, upon convolution of the simulated peaks with the experimental broadening we obtain a nearly perfect resemblance of the experiment. This is nicely reflected in the formation of special features in the spectra, e.g., the sharp ridge at −7.8 eV in the Fig. 4(f) spectra that can be found in both experiment and simulations. Simulations for an energy value detuned by −2 eV from the resonance position, where we have no experimental data for comparison, show that for this hypothetical detuning, the spectator band at 0 eV collapses completely and only a single elastic scattering line remains, whereas the spectator final states are always formed by bands of multiple vibrationally excited states.

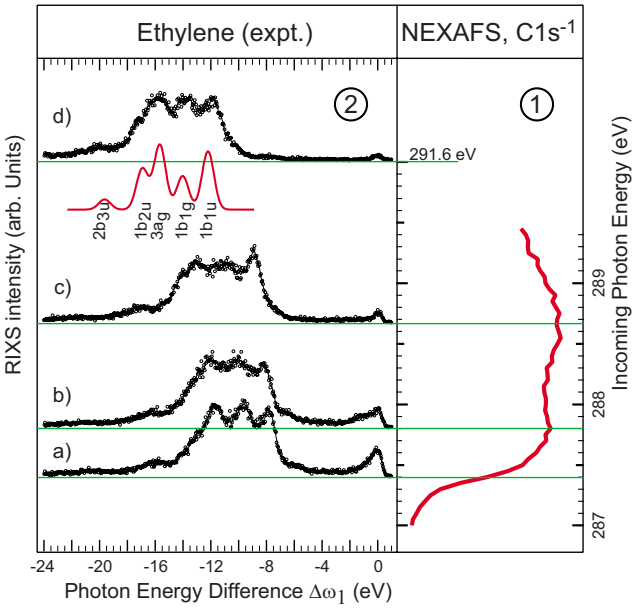

FIG. 5. (Color online) RIXS of ethylene at the C*K* edge in the Rydberg region. Panel (1): Absorption spectrum; (2): RIXS spectra (exp.) with excitation at the energies indicated, plotted vs the energy difference of outgoing and incoming photon $\Delta\omega_1 = \omega_1 - \omega$. The inset shows nonresonant calculations from Ref. [41]. The spectra are arbitrarily scaled to equal maximum height.

We now turn to scattering at energies in the Rydberg or continuum region (Fig. 5). A comparison of the higher energy region in the XAS (Fig. 3) with data published by Gadea *et al.* [23], Rabus *et al.* [42] shows significant differences between gas phase and condensed ethylene. Our spectra agree with the condensed measurements published before [40]. In the region above 287 eV, the gas-phase molecules show several discrete resonances, whereas in the condensed case only two very broad states remain. The Rydberg states here overlap due to van der Waals interaction of the closed packed molecules and the fine structure quenches and broadens [43]. RIXS spectra measured after excitation into the Rydberg region are depicted in Fig. 5, panel 2. The excitation energies are indicated in the XA spectrum in panel 1 by the horizontal lines.

The participator peak (Fig. 5) around $\Delta\omega_1 = 0$ eV is at first (a) quite strong, although weaker as on resonant excitation into the π^*. The reason for this is to be found in the smaller overlap of the Rydberg orbitals with the C 1*s* wave function in comparison with large overlap $\langle \pi^* | \mathbf{r} | 1s \rangle$ between 1*s* and the LUMO. With increasing excitation energy the intensity of this peak then decreases due to the decrease of the transition matrix element for higher Rydberg states. Exciting detuned (a), the peak is clearly asymmetric and on top of the first resonance (b), the formation of a second band centered at ≈−0.6 eV can be seen. After increasing the excitation energy further it again becomes symmetric. This is a clear evidence for participator contribution into this feature, in contrast to a pure inelastic scattering process.

For a tentative assignment of the emission from the valence orbitals, respectively, scattering into electronically excited final states, we have inserted purely electronic XES

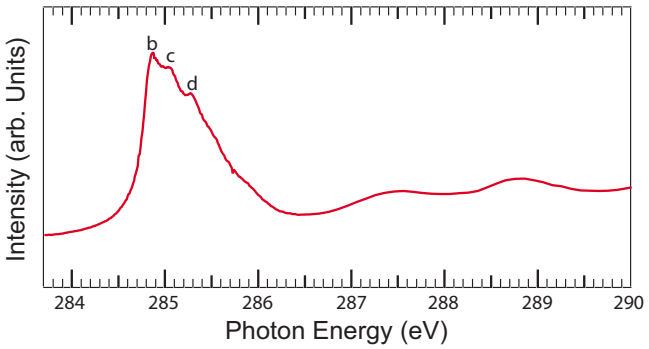

FIG. 6. (Color online) X-ray absorption spectrum of condensed benzene.

calculations of gas-phase ethylene from Ref. [41]. We observe emission from the $2b_{3u}$, $1b_{2u}$, $3a_g$, $1b_{1g}$, and $1b_{1u}$ electronic orbitals, roughly equally strong for all excitation energies. The experimental spectra show only weak excitation energy dependence and resemble the nonresonant calculations as well as the nonresonant x-ray emission spectrum (XES) of ethylene [14] very closely. The only remarkable difference can be found in the intensity of the $1b_{1g}$, which is stronger here in the condensed layer measurements compared to both calculations [41] and experiment [14] in the gas-phase case. This orbital can also be denoted as the π_{CH_2} orbital and accounts for the CH bonding. Tuning the excitation energy into the rising flank (a) of the Rydberg region, all final states are well separated. Scattering on top of the two broad resonances, these final states broaden and smear out, while after excitation above (d) they again separate. When exciting at the second broad resonance (c), the emission from the $1b_{1u}$ orbital is found to be slightly enhanced above the others.

B. Benzene

The benzene molecule has D_{6h} symmetry and its electronic configuration in the ground state is

$$\text{Core: } (1a_{1g})^2(1e_{1u})^4(1e_{2g})^4(1b_{2u})^2 = \psi_{\text{core}},$$

$$\text{Valence: } (2e_{1u})^4(2e_{2g})^4(3a_{1g})^2(2b_{1u})^2(1b_{2u})^2 \times (3e_{1u})^4(1a_{2u})^2(3e_{2g})^4(1e_{1g})^4.$$

The HOMO ($1e_{1g}$) is a π orbital. The lowest unoccupied molecular orbital ($1e_{2u}$) has π^* character.

Carbon *K*-edge XAS of condensed benzene is presented in Fig. 6. As in ethylene, we can separate the resonance with a maximum at 284.85 eV and a higher energy region with two broad features around 287.5 eV and 288.8 eV. We again discuss the resonance region first. We compared the spectra to XAS reported for condensed [40] and free [44] benzene with similar result as for ethylene. The shape of the C $1s \rightarrow \pi^*(1e_{2u})$ resonance agrees for condensed and gas phase with our measurement, backing our preparation and the model function of the condensate for the isolated molecule in the π^* resonance region. Our spectrum resolves all reported

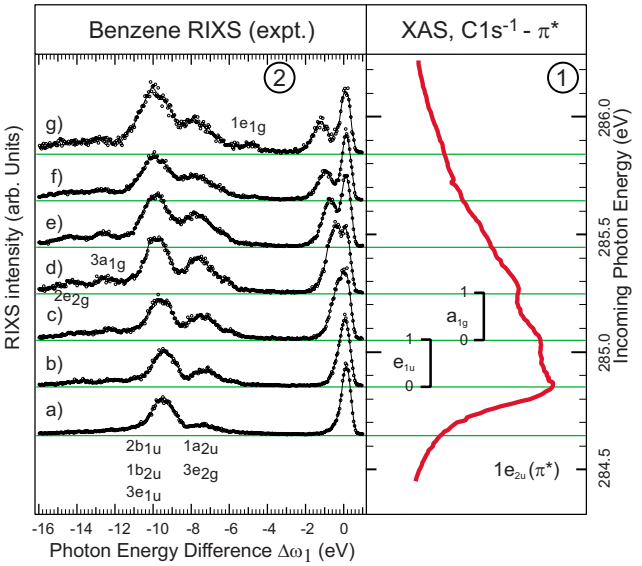

FIG. 7. (Color online) RIXS of benzene at the C*K* edge in the region of the C $1s \rightarrow \pi^*$ resonance. Panel (1): Absorption spectrum with partly assigned vibrational states; (2): RIXS spectra (exp.) with excitation at the energies indicated. RIXS spectra are plotted vs the energy difference of outgoing and incoming photon $\Delta\omega_1 = \omega - \omega$. The spectra are arbitrarily scaled to equal maximum height.

features except for a small state right above the absorption maximum reported by Ma *et al.* [40]. The fine structure represents the vibrational progression of the π^* resonance. Following the discussion summarized by Rennie *et al.* [44], we can assign (b) to the $0 \rightarrow 0$ transition and (c) to a e_{1g} CH bend and to an e_{1u} ring stretch and deformation. (d) combines the former modes with an a_{1g} C-H stretch mode.

Figure 7 shows the resonant scattering data for condensed benzene. For comparison, we again show the XA spectrum in panel 1 and indicate the excitation energies with horizontal lines. The spectral distribution of the outgoing photons changes strongly with excitation energy. For scattering into the electronic ground state, we observe a behavior very similar to ethylene. Excitation detuned from the electronic resonance (a) gives rise to a single, slightly asymmetric peak at 0 eV (elastic peak). The 0 eV feature broadens and becomes more asymmetric when tuning the excitation energy on top of the resonance (b) and into the first level of the vibrational progression (c). Upon excitation with higher energies [lines (d)–(g)], it splits into two contributions, one staying at 0 eV and one moving toward lower energies similar to the ethylene case. The intensity of the moving fraction decreases with increasing excitation energy. The region of valence excited final states between −16 eV and −3 eV were compared to data published [16] and electronic simulations from Ref. [41] for a tentative assignment of the spectral features as labeled in the plot. Due to the multitude of valence orbitals in benzene, these features convolute several final states.

According to dipole selection rules applying for the absorption of a photon only a core hole in orbital $1e_{2g}$ can be created under excitation of a core electron into the LUMO $1e_{2u}$. Emission transitions filling this particular core vacancy are only allowed from the occupied MOs $2e_{1u}$, $2b_{1u}$, $1b_{2u}$,

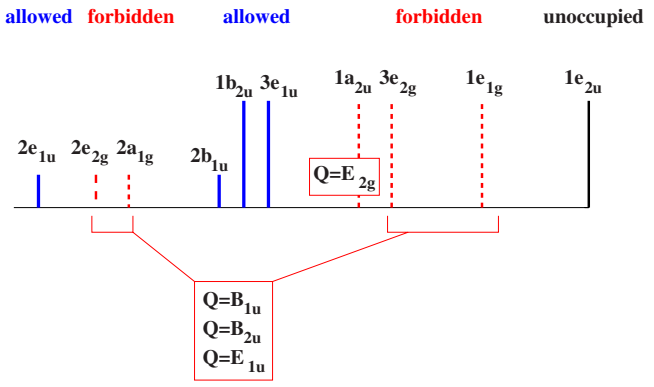

FIG. 8. (Color online) Scheme of allowed RIXS transitions in benzene under core excitation into the LUMO $\pi^*(1e_{2u})$. Dashed lines show symmetry forbidden transitions, which become allowed by vibronic coupling after excitation of the indicated vibrational modes Q.

and $3e_{1u}$. However, due to vibronic coupling these pure electronic selection rules are over-ruled: The activation of vibrational modes with b_{1u}, b_{2u}, and e_{1u} symmetry "opens" transition channels from the occupied MOs $2e_{2g}$, $3a_{1g}$, $3e_{2g}$, $1e_{1g}$, while coupling to mode e_{2g} allows the emission transition from the $1a_{2u}$ MO (see Fig. 8). Exciting detuned from the resonance (a), we see two broad peaks: The first at −9.4 eV we assign to the $|1b_{2u}^{-1}1e_{2u}\rangle$, $|2b_{1u}^{-1}1e_{2u}\rangle$ and $|3e_{1u}^{-1}1e_{2u}\rangle$ final states, the other peak at −7.4 eV is assigned to $|1a_{2u}^{-1}1e_{2u}\rangle$ and $|3e_{2g}^{-1}1e_{2u}\rangle$. Upon excitation on top of the resonance (b) and with higher energies [lines (c)–(g)], these two features change their shape and width and their relative intensity ratio. The states represented by these features show different excitation energy dependence; the changes in peak shape and in relative intensity reflect this. Upon resonant excitation into the vibrational progression [lines (b)–(g)], additional features show up. They increase in relative intensity to the other features with increasing excitation energy. We assign the features at −14.4 eV to $|2e_{2g}^{-1}1e_{2u}\rangle$, at −12.6 eV to $|3a_{1g}^{-1}1e_{2u}\rangle$ and at −5 eV to $|1e_{1g}^{-1}1e_{2u}\rangle$. The intensity ratio between the peaks at −9.4 eV and −7.4 eV is roughly 4:1 below resonance (a). On top (b) and above resonance [lines (c)–(g)], the peak at −7.4 eV gains relative intensity and the ratio alters to about 2:1. In agreement with the increasing intensity at −7.4 eV, we conclude that this intensity change reflects an increase of scattering into the "electronic symmetry forbidden" $|1a_{2u}^{-1}1e_{2u}\rangle$ and $|3e_{2g}^{-1}1e_{2u}\rangle$ final states.

The higher energy part of the XAS spectra (Fig. 6 and Fig. 9, panel 1) reflects the condensed case [45] missing some fine structure visible in the gas phase [44]. Comparing to Rennie *et al.* [44] we assign the peak at 287.5 eV to the broadened $3s$ Rydberg state and the peak at 288.8 eV to the $\pi^*(1b_{2g})$ excitation. In benzene, the ionization potential lowers below the C-H* resonance [43].

RIXS under excitation into the Rydberg states is displayed in Fig. 9. The inset shows nonresonant XES calculations [41] of the gas-phase case in the adiabatic limit neglecting changes in the vibrational wave function and allowing for a tentative assignment of the spectral features. In benzene, stronger variations of the relative intensity of the peaks with

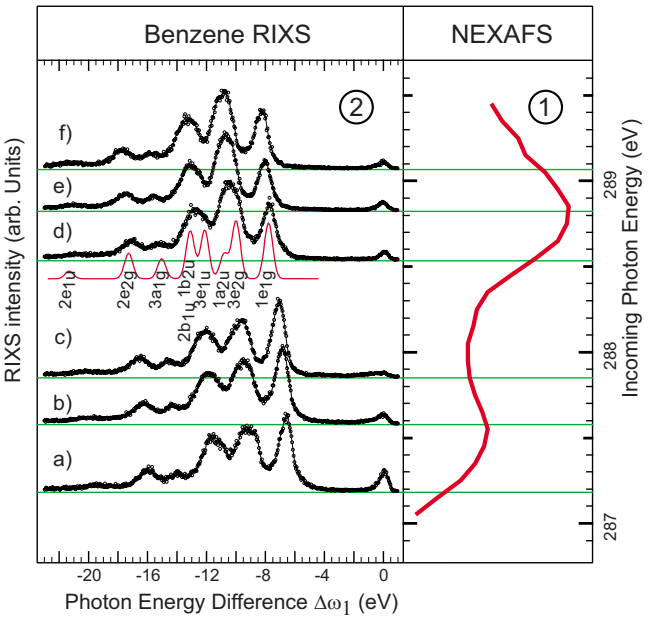

FIG. 9. (Color online) RIXS of benzene at the CK edge in the Rydberg region. Panel (1): Absorption spectrum; (2): RIXS spectra (exp.) with excitation at the energies indicated, plotted vs the energy difference of outgoing and incoming photon $\Delta\omega_1=\omega_1-\omega$. The inset shows nonresonant calculations from Ref. [41]. The spectra are arbitrarily scaled to equal maximum height.

the excitation energy can be observed as compared to ethylene, whereas the separation and width of the features do not change noticeable. Upon excitation into the region of the $3s$ Rydberg resonance at 287.5 eV [lines (a)–(c)], the π $(1e_{1g})$ peak at −7 eV is enhanced compared to the other features and compared to the nonresonant gas-phase calculations. Exciting around the $\pi^*(1b_{2g})$ resonance at 288.8 eV, the peak at −9 eV $(1a_{2u}$ or $3e_{2g})$ is enhanced over the others and compared to the calculations.

V. DISCUSSION

Both ethylene and benzene show very similar effects in the RIXS. We will jointly discuss both molecules to work out the analogies and differences. The RIXS scattering depends strongly on the excitation energy. In the π^* resonance region, even small variations of the incident photon energy have big influence on the scattering profile. In the energy region >2 eV above the resonance, the variations are smaller but still significant. The simulations cover the region of the absorption resonance only. We will first evaluate the π^* region and then discuss how the interpretation can be extended to the region of continuum excitation. The scattering simulations reflect the experimental data in high detail. In the following discussion, we will, thus, jointly discuss both data sets and not distinguish between experiment and calculations.

A. Dynamics of x-ray Raman scattering

In both the participator region of scattering into the electronic ground state and the spectator region of valence elec-

tronically excited final states we observe strong excitation energy dependences. To understand the differences underlying detuned and resonant scattering we invoke the scattering duration time concept [3,46]. The duration time τ of the scattering process is defined by [48]

$$\tau = 1 \Big/ \sqrt{\Omega^2 + \left(\frac{\Gamma}{2}\right)^2}. \tag{10}$$

Here Ω is the detuning of the excitation energy (ω) from the top of photoabsorption. The time scale of the nuclear motion is defined by the period of vibration $2\pi/\omega_q$. In the limit of large detuning Ω the total scattering time becomes very short, effectively not leaving time for the vibrational wave packet to evolve in the scattering intermediate state. In this case, excitation and decay follow each other suddenly and the nuclei cannot move in between. In the immediate decay after excitation, the initial probability density of the ground state is unchanged projected on the final state. This is equivalent to a direct transition from the initial to the final state. In other words, large detuning Ω (or large lifetime broadening) corresponds to fast Raman scattering.

This effect is reflected in the asymptotic expression for the scattering amplitude (8) in the limit of fast scattering [3,34,35]:

$$\mathcal{F}_{\nu_f} \approx \frac{\langle \nu_f | 0_0 \rangle}{2(\Omega + {}_1\Gamma/2)}(1 + \mathcal{P}_f), \quad \tau\omega_q \ll 1, \tag{11}$$

here valid for molecules with two equivalent atoms. The general expression for the resonant x-ray Raman scattering amplitude (2) in the limit of fast scattering is

$$F_{\nu_f} \approx \frac{\langle \nu_f | 0_0 \rangle}{\Omega + {}_1\Gamma/2} \langle f | (\mathbf{e}_1 \cdot \mathbf{r})\,(\mathbf{e} \cdot \mathbf{r}) | 0 \rangle, \quad \tau\omega_q \ll 1. \tag{12}$$

In general the fast scattering is not affected by vibronic coupling in the core excited state and the scattering follows to the electronic selection rules for the scattering tensor. These selection rules are given by the quadrupole operator $(\mathbf{e}_1 \cdot \mathbf{r})(\mathbf{e} \cdot \mathbf{r})$ in the matrix element between ground and final electronic states.

Thus, in the case of detuned excitation (fast scattering), the formation of the spectrum can be understood as a result of a direct Franck-Condon transition from the ground state to the final state, $\langle \nu_f | 0_0 \rangle$, because the nuclear wave packet in core excited state has not time to spread during the scattering: $|\psi(t)\rangle \approx |0_0\rangle$. For the limit of fast scattering we can now distinguish different effects in the participator or "elastic" channel and the spectator or "inelastic" channel. In the participator decay the final state is the electronic ground state. The potential surfaces of initial and final state strictly coincide and according to the Franck-Condon principle only a single line corresponding to the $0 \rightarrow 0$ transition is observed $\langle \nu_f | 0_0 \rangle = \delta_{\nu_f, 0_0}$. This is the so-called collapse effect [3,35]. For the valence excited final states in the spectator channel, the potential surfaces of the ground and final states do not generally coincide. Except for the special case where they do, transitions into vibrationally excited states are always possible, $\langle \nu_f | 0_0 \rangle \neq \delta_{\nu_f, 0_0}$.

On resonant excitation $\Omega = 0$, the scattering duration time τ becomes sufficiently large for the nuclei to move on the potential surface of the core excited intermediate state. Now the nuclear wave packet in core excited state has time to spread and it differs from the initial wave packet: $|\psi(t)\rangle \neq |0_0\rangle$. In this case scattering through the intermediate vibrational levels $|\nu_i\rangle$ of the core excited state becomes important and the scattering spectral profile (i.e., the intensity of the observed spectral features) is affected strongly by channel interference between scattering over different vibrationally excited intermediate states.

B. Vibronic coupling

So far we have discussed the change in shape and width of the vibrational bands belonging to a specific electronic final state as a function of excitation energy. In both systems, ethylene and benzene, we see an additional effect which we have not yet accounted for. In both molecules additional valence excited final states show up upon excitation into higher lying states of the LUMO's vibrational progression. These are the electronic symmetry forbidden *ungerade* final states $|1b_{1u}^{-1}1b_{2g}\rangle$ and $|1b_{2u}^{-1}1b_{2g}\rangle$ in the case of ethylene and the final states $|2e_{2g}^{-1}1e_{2u}\rangle$, $|3a_{1g}^{-1}1e_{2u}\rangle$, $|1a_{2u}^{-1}1e_{2u}\rangle$, $|3e_{2g}^{-1}1e_{2u}\rangle$, and $|1e_{1g}^{-1}1e_{2u}\rangle$ in case of benzene. To explain this behavior we turn to the discussion of the selection rules applicable for electronic transitions. If only the electronic wave function is considered, the x-ray Raman scattering would follow the selection rules for the scattering tensor [3]. In the case of the ethylene molecule scattering is only allowed into those final states where the total parity of the electronic wave function is not changed with respect to the ground state. Since the ground state is totally symmetric and has *gerade* parity, only *gerade* final states would be allowed. In ethylene this is the case for the $|1b_{1g}^{-1}1b_{2g}\rangle$ and the $|3a_g^{-1}1b_{2g}\rangle$ final states. In the case of benzene (D_{6h} group) the selection rules are different [3] and scattering is symmetry forbidden into the *ungerade* and some *gerade* final states (as discussed above). The allowed final states are $|2e_{1u}^{-1}1e_{2u}\rangle$, $|2b_{1u}^{-1}1e_{2u}\rangle$, $|1b_{2u}^{-1}1e_{2u}\rangle$, and $|3e_{1u}^{-1}1e_{2u}\rangle$.

Nevertheless, the experiment shows also resonant scattering into the final states that are "symmetry forbidden." The reason for this is the vibronic coupling mixing electronic core excited states with different symmetries when the appropriate vibrational modes are activated. The core excitation into these symmetry forbidden core excited states opens new emission channels. However, both experiment and theory show that such a "symmetric breaking" happens only when the photon frequency ω is tuned close to a symmetry breaking vibrational mode. In the limit of large detuning $|\Omega|$ we converge to the case of pure electronic selection rules. This can easily be understand for the special case of ethylene from Eq. (11), because there the scattering amplitude vanishes ($\mathcal{F}_{\nu_f} = 0$) for all *ungerade* final states $f = u$. This equation demonstrates the general phenomenon, a restoration of the electronic selection rules in fast scattering [given by general expression for the RXRS amplitude of fast scattering (12)]. The effect is confirmed nicely by both experiment and simulations.

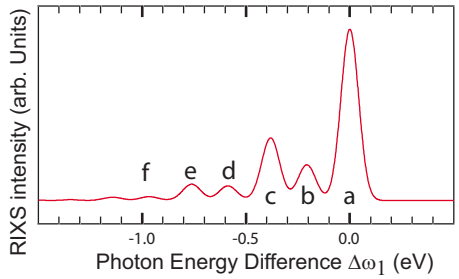

FIG. 10. (Color online) Participator channel: Purely vibrational inelastic x-ray scattering (soft x-ray vibrational Raman) at C_2H_4 at the π resonance maximum at 284.37 eV (compare Fig. 4). The vibrational modes 3, 4, and 5 (Table II) contribute to the spectra: (a) $0\rightarrow 0$; (b) $\nu_5(0\rightarrow 1)$; (c) 93% $\nu_3(0\rightarrow 1)$/7% $\nu_5(0\rightarrow 2)$; (d) $\nu_3(0\rightarrow 1)+\nu_5(0\rightarrow 1)$; (e) 69% $\nu_3(0\rightarrow 2)$/20% $\nu_4(0\rightarrow 2)$/11% $[\nu_3(0\rightarrow 1)\nu_5(0\rightarrow 2)]$; (f) $\nu_3(0\rightarrow 2)+\nu_5(0\rightarrow 1)$.

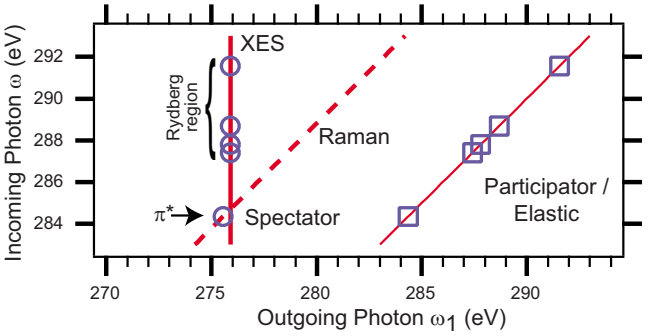

FIG. 11. (Color online) Schematic plot of the energy dispersion of spectator and participator and/or elastic contribution. The markers indicate the experimentally observed position of the participator (squares) and the $3a_g$ (circles) in ethylene (Figs. 4 and 5) as an example. The dashed line represents Raman dispersion, the thick solid line fixed emission energy (XES).

This process of vibronic coupling upon resonant excitation and "sharpening" of the selection rules is to be understood as a dynamic process. If the scattering duration (10) is sufficiently large—as it is the case in resonant excitation—the symmetry breaking vibrations have enough time to distort the molecule to a nonsymmetric configuration, where the core excited states are no longer represented in the ground state symmetry of the molecule and, thus, the selection rules can no longer operate on the delocalized representations. When we detune from resonant excitation, the scattering duration becomes too short for the vibrations to change symmetry. In a sudden scattering process, the molecular configuration symmetry and, thus, the according selection rules are conserved.

C. Purely vibrational and vibronic Raman

From the discussed dynamics of x-ray Raman scattering we see that upon resonant core excitation vibrationally excited final states can be observed in the participator channel. There we, thus, observe purely vibrational Raman loss features in the soft x-ray regime, resonantly enhanced when tuning into a molecular resonance. As it is the case for the vibrational loss features in ordinary optical Raman spectroscopy, this gives access to the electronic ground state potential energy surfaces through the vibrational progression. However, resonance excitation at core level with x-rays gives additional atom specific and chemical state selective sensitivity and the local potential energy surface can be associated to specific atomic centers and chemical environments. This observation of purely vibrational states is in principal possible only in a photon-in-photon-out spectroscopy, where electronically not excited final states can be reached. In Fig. 10 we show a detail of the calculated RIXS spectra of ethylene. The participator band consists of distinct vibrational lines. Only the peak at 0 eV corresponds to elastic scattering. The mode analysis reveals that only those final states are active in the scattering, where the parity of the total wave function is conserved.

The spectator region, corresponding to scattering into electronically excited final states, contains combined electronic and vibrational loss features. In the spectator channel, we, thus, probe the vibrational properties of valence excited final states.

D. Rydberg and continuum region

RIXS of ethylene (Fig. 5) and benzene (Fig. 9) in the Rydberg and continuum region roughly resemble the nonresonant XES spectra. Here the clear symmetry effects in RIXS cannot be observed. The main reason for this is the small spacing between *gerade* and *ungerade* Rydberg (as well as continuum) states. Due to this the scattering does not display the selection rules because core holes of either symmetry are created with comparable probability.

Comparison of the spectra for Rydberg or continuum excitation (Figs. 5 and 9) with the spectral profiles (Figs. 4 and 7) near core excitation into the LUMO shows a smaller relative intensity of the participator or "elastic" band in the case of excitation of Rydberg or continuum states. The intensity ratio of elastic and inelastic bands is given by the square of the ratio of absorption and emission transition dipole moments d_{i0}^2/d_{fi}^2. This ratio is small for Rydberg states because these states are more diffuse compared to the LUMO. This explains also why the elastic peak is smaller for higher Rydberg states.

E. Energy dispersion

We finally discuss the energy position of the spectral lines. The energy dispersion of the spectra is different for resonant excitation near the LUMO and excitation in the Rydberg region. If we only consider the $0\rightarrow 0$ vibrational transition in the participator band, this feature follows the Raman dispersion law $\sigma_{el}(\omega,\omega_1)\propto\delta(\omega_1-\omega)$ in nice agreement between theory and experiment (Fig. 11).

In the case of excitation into the Rydberg region the center of gravity of the inelastic or spectator band is not dispersive similar to the off-resonant emission (XES) [3]. Our simulations show that the dispersion of this band upon excitation near the LUMO is more complicated because the cen-

ters of gravity of different vibrational subbands exhibit different dispersions. They are referred to as "vertical" and "resonant" bands in Ref. [49]. We see from both theory and experiment that the center of gravity of the RIXS features follows a nonlinear dispersion under excitation near the LUMO. Nevertheless our simulations show that each single vibrational state still follows linear dispersion and can thus be identified as a Raman feature.

VI. SUMMARY

We have experimentally observed and theoretically described purely vibrational and vibronic Raman scattering in RIXS for vibrationally selective excitation.

In both model systems, ethylene and benzene, pure vibrational loss processes were identified. The energy positions of these spectral features reflect through their vibrational progression the local potential energy surface of the system in the electronic ground state at the atomic site of excitation. In addition, the femtosecond intermediate state dynamics is reflected by the relative intensity distribution within the vibrational progression. Intermediate state interference effects between scattering paths involving different vibrationally excited intermediate states can be observed. The nature of the scattering process changes significantly with the duration time of the scattering. On resonant excitation, indeed, even in the soft x-ray regime, the scattering duration becomes sufficiently large to probe nuclear dynamics with RIXS and electronic ground state potential energy surfaces around selected atomic sites can be studied.

Scattering into electronically excited final states is found to be always accompanied by vibrational excitations. Furthermore, upon resonant excitation vibronic coupling is observed, leading to interference between equivalent core hole localization channels. This opens scattering into additional final states. Thus the interpretation of molecular systems under resonant excitation needs careful consideration of all of the described coupled electronic and vibrational processes. With the advanced theoretical and computational treatment presented here we are able to fully describe these processes and model the resonant vibrational and vibronic Raman scattering for the model system of ethylene.

ACKNOWLEDGMENTS

This work was supported by the Access to Research Infrastructure (ARI) Program, the Swedish National Research Council (VR), and the Deutsche Forschungsgemeinschaft (Grant No. DFG Fo343/1-1). M.N. acknowledges support of a part of this work by "MEXT Japan, Grant in aid for Young Scientists (B) 2003." Valuable support from Lisbeth Kjeldgaard and the MAX-lab staff is gratefully acknowledged.

[1] A. Föhlisch, M. Nyberg, J. Hasselström, O. Karis, L. G. M. Pettersson, and A. Nilsson, Phys. Rev. Lett. **85**, 3309 (2000).
[2] J. Nordgren and J. Guo, J. Electron Spectrosc. Relat. Phenom. **110-111**, 1 (2000).
[3] F. Gel'mukhanov and H. Ågren, Phys. Rep. **312**, 87 (1999).
[4] A. Kotani and S. Shin, Rev. Mod. Phys. **73**, 203 (2001).
[5] L. Triguero, Y. Luo, L. G. M. Pettersson, H. Ågren, P. Väterlein, M. Weinelt, A. Föhlisch, J. Hasselström, O. Karis, and A. Nilsson, Phys. Rev. B **59**, 5189 (1999).
[6] J. Nordgren, P. Glans, K. Gunnelin, J. Guo, P. Skytt, C. Såthe, and N. Wassdahl, Appl. Phys. A **65**, 97 (1997).
[7] A. Nilsson and L. G. M. Pettersson, Surf. Sci. Rep. **55**, 49 (2004).
[8] A. Föhlisch, J. Hasselström, P. Bennich, N. Wassdahl, O. Karis, A. Nilsson, L. Triguero, M. Nyberg, and L. G. M. Pettersson, Phys. Rev. B **61**, 16229 (2000).
[9] L. Triguero, A. Föhlisch, P. Väterlein, J. Hasselström, M. Weinelt, L. G. M. Pettersson, Y. Luo, H. Ågren, and A. Nilsson, J. Am. Chem. Soc. **122**, 12310 (2000).
[10] Y. Ma, P. Skytt, N. Wassdahl, P. Glans, D. C. Mancini, J. Guo, and J. Nordgren, Phys. Rev. Lett. **71**, 3725 (1993).
[11] Y. Harada, T. Tokushima, Y. Takata, T. Takeuchi, Y. Kitajima, S. Tanaka, Y. Kayanuma, and S. Shin, Phys. Rev. Lett. **93**, 017401 (2004).
[12] P. Skytt, P. Glans, K. Gunnelin, J. Guo, and J. Nordgren, Phys. Rev. A **55**, 146 (1997).
[13] P. Glans, P. Skytt, K. Gunnelin, J. H. Guo, and J. Nordgren, J. Electron Spectrosc. Relat. Phenom. **82**, 193 (1996).
[14] K. Gunnelin, P. Glans, J.-E. Rubensson, C. Såthe, J. Nordgren, Y. Li, F. Gel'mukhanov, and H. Ågren, Phys. Rev. Lett. **83**, 1315 (1999).
[15] P. Skytt, P. Glans, J.-H. Guo, K. Gunnelin, C. Såthe, J. Nordgren, F. K. Gel'mukhanov, A. Cesar, and H. Ågren, Phys. Rev. Lett. **77**, 5035 (1996).
[16] P. Skytt, J. Guo, N. Wassdahl, J. Nordgren, Y. Luo, and H. Ågren, Phys. Rev. A **52**, 3572 (1995).
[17] J.-H. Guo, Y. Luo, A. Augustsson, S. Kashtanov, J.-E. Rubensson, D. K. Shuh, H. Ågren, and J. Nordgren, Phys. Rev. Lett. **91**, 157401 (2003).
[18] P. Wernet *et al.*, Science **304**, 995 (2004).
[19] J.-H. Guo, Y. Luo, A. Augustsson, J.-E. Rubensson, C. Såthe, H. Ågren, H. Siegbahn, and J. Nordgren, Phys. Rev. Lett. **89**, 137402 (2002).
[20] F. Hennies, S. Polyutov, I. Minkov, A. Pietzsch, M. Nagasono, F. Gel'mukhanov, L. Triguero, M.-N. Piancastelli, W. Wurth, H. Agren, and A. Föhlisch, Phys. Rev. Lett. **95**, 163002 (2005).
[21] P. Jakob and D. Menzel, Surf. Sci. **220**, 70 (1989).
[22] S. G. J. Mochrie, M. Sutton, R. J. Birgeneau, D. E. Moncton, and P. M. Horn, Phys. Rev. B **30**, 263 (1984).
[23] F. X. Gadea, H. Köppel, J. Schirmer, L. S. Cederbaum, K. J. Randall, A. M. Bradshaw, Y. Ma, F. Sette, and C. T. Chen, Phys. Rev. Lett. **66**, 883 (1991).
[24] R. Denecke, P. Väterlein, M. Bässler, N. Wassdahl, A. Nilsson, J.-E. Rubensson, J. Nordgren, N. Mårtensson, and R. Nyholm, J. Electron Spectrosc. Relat. Phenom. **101-103**, 971 (1999).
[25] D. Menzel, G. Rocker, H.-P. Steinrück, D. Coulman, P. A. Heimann, W. Huber, P. Zebisch, and D. R. Lloyd, J. Chem.

Phys. **96**, 1724 (1992).
[26] M. N. Piancastelli, W. C. Stolte, G. Öhrwall, S.-W. Yu, D. Bull, K. Lantz, A. S. Schlachter, and D. W. Lindle, J. Chem. Phys. **117**, 8264 (2002).
[27] F. Gel'mukhanov and H. Ågren, J. Electron Spectrosc. Relat. Phenom. **93**, 31 (1998).
[28] F. Gel'mukhanov and H. Ågren, Phys. Rev. A **49**, 4378 (1994).
[29] P. Salek, A. Baev, F. Gel'mukhanov, and H. Ågren, Phys. Chem. Chem. Phys. **5**, 1 (2003).
[30] H. Köppel, W. Domcke, and L. S. Cederbaum, Adv. Chem. Phys. **57**, 59 (1984).
[31] K. J. Børve, L. J. Sæthre, T. D. Thomas, T. X. Carroll, N. Berrah, J. D. Bozek, and E. Kukk, Phys. Rev. A **63**, 012506 (2000).
[32] H. A. Kramers and W. Heisenberg, Z. Phys. **31**, 681 (1925).
[33] F. K. Gel'mukhanov, L. N. Mazalov, and A. V. Kondratenko, Chem. Phys. Lett. **46**, 133 (1977).
[34] F. Gel'mukhanov, T. Privalov, and H. Ågren, Zh. Eksp. Teor. Fiz. **112**, 37 (1997) [JETP **85**, 20 (1997)]
[35] F. Gel'mukhanov, T. Privalov, and H. Ågren, Phys. Rev. A **56**, 256 (1997).
[36] P. Salek, F. Gel'mukhanov, and H. Ågren, Phys. Rev. A **59**, 1147 (1999).
[37] StoBe-deMon version 1.0, K. Hermann, L. G. M. Pettersson, M. E. Casida, C. Daul, A. Goursot, A. Koester, E. Proynov, A. St-Amant, D. R. Salahub. Contributing authors: V. Carraveta, H. Duarte, N. Godbout, J. Guan, C. Jamorski, M. Leboeuf, V. Malkin, O. Malkina, M. Nyberg, L. Pedocchi, F. Sim, L. Triguero, A. Vela, StoBe Software, 2002.
[38] T. Karlsen, L. J. Sæthre, K. J. Børve, N. Berrah, E. Kukk, J. D. Bozek, T. X. Carroll, and T. D. Thomas, J. Phys. Chem. A **105**, 7700 (2001).
[39] K. C. Prince, M. Vondrek, J. Karvonen, M. Coreno, R. Camilloni, L. Avaldi, and M. de Simone, J. Electron Spectrosc. Relat. Phenom. **101-103**, 141 (1999).
[40] Y. Ma, F. Sette, G. Meigs, S. Modesti, and C. T. Chen, Phys. Rev. Lett. **63**, 2044 (1989).
[41] L. Triguero, L. Pettersson, and H. Ågren, J. Phys. Chem. A **102**, 10599 (1998).
[42] H. Rabus, D. Arvanitis, M. Domke, A. Puschmann, L. Wenzel, C. Comelli, G. Kaindl, and K. Baberschke, Phys. Scr., T **31**, 131 (1990).
[43] J. Stöhr, *NEXAFS Spectroscopy* (Springer, Berlin, 1992).
[44] E. E. Rennie *et al.*, J. Chem. Phys. **113**, 7362 (2000).
[45] J. Solomon, R. Madix, W. Wurth, and J. Stöhr, J. Phys. Chem. **95**, 3687 (1991).
[46] The off-resonant suppression of long-time contributions in optical Raman spectroscopy was observed earlier [47] using direct time resolved measurements.
[47] P. F. Williams, D. L. Rousseau, and S. H. Dworetsky, Phys. Rev. Lett. **32**, 196 (1974).
[48] We here correctly refer to Γ as full width half maximum. In our former publication [20] we used the equation for Γ defined as half width half maximum, thus being inconsistent with the rest of our discussion there.
[49] R. Feifel *et al.*, Phys. Rev. A **69**, 022707 (2004).